Supporting Materials

Construction of photonic radiative cooling layer based on 3D conductive network foam for efficient electromagnetic interference shielding and environmental thermal comfort

Mingtai Liu, Hongjian Huang*, Jie Mei, Siqi Yang*, Hao Tu, Jian Wang*

Key Laboratory of materials and surface technology (Ministry of Education), School of Materials Science and Engineering, Xihua University, Chengdu 610039, People's Republic of China

*Corresponding author.

E-mail address: wangjianxhu@163.com (Jian Wang)

Postal address: No. 999 Jinzhou Road, Chengdu 610039, People’s Republic of China

Materials

MF was purchased from Shanghai Beiyou Construction Materials Co., Ltd., China. Aramid paper was acquired from DuPont, USA. Pyrrole (C_4H_5N) was bought by Macklin Biochemica Technology Co., Ltd., Shanghai, China. Polydimethylsiloxane (PDMS) and the curing agent were procured by Dow Corning Corporation, USA. High purity Al_2O_3 powder was purchased from Hebei Juli Metal Material Co., Ltd., China. Conductive silver paint was purchased from the Shenzhen Jingche Technology Enterprise Shop. Ammonia ($NH_3{\cdot}H_2O$), ferric chloride ($FeCl_3{\cdot}6H_2O$), ferrous sulfate ($FeSO_4{\cdot}7H_2O$), ethyl acetate ($C_4H_8O_2$) was acquired uniformly from Chengdu Kelong Chemicals Co., Ltd., China. Deionized water for experiments was prepared by Q-20C purification system.

Characterization

The micromorphology and elemental mapping of samples were investigated with field emission scanning electron microscope (FE-SEM, ZEISS Gemini 300, Germany) and energy dispersive spectrometer (EDS, Smarted X). An X-ray diffractometer (XRD, Rigaku SmartLab SE, Japan) was applied to characterize the crystal structure of samples. The electrical conductivity and magnetic properties of the samples were determined by the four-probe method (ST2643F and ST2258C) and vibrating sample magnetometer (VSM, Lake Shore 7404, USA). Optical reflectance (R) and transmittance (T) of the samples were measured in the range of 200-2500 nm using a UV-Visible Near Infrared Spectrophotometer (Japan-Shimadzu-UV-3600 plus). The infrared thermal emissivity was collected by a Fourier infrared spectrometer (Bruker invenio s) with a measurement range of 2.5-25 μm. Full-spectrum metal halide lamp (UVB, Huizhou Jinke Lighting Technology Co.) was used to provide simulated sunlight. A solar power meter pyranometer (TES 132) was used to measure the light intensity of the sunlight. A vector network analyzer (Agilent PNA-N5234A-USA) was used to acquire the S-parameters of the samples by the waveguide method. The total shielding effectiveness (SE_T), reflection shielding effectiveness (SE_R), absorption shielding effectiveness (SE_A), multiple reflection shielding (SE_M) and the power coefficient of absorption (A), reflection (R) and transmission (T) were calculated as follows:

$$R = |S_{11}|^2, T = |S_{21}|^2 \quad (1)$$

$$A = 1 - R - T \quad (2)$$

$$SE_A = -10\lg\left(|S_{21}|^2/\left(1 - |S_{11}|^2\right)\right) = -10\lg\left(T/(1 - R)\right) \quad (3)$$

$$SE_R = -10\lg\left(1 - |S_{11}|^2\right) = -10\lg\left(1 - R\right) \quad (4)$$

$$SE_T = SE_A + SE_R + SE_M \quad (5)$$

In general, SE_M is negligible when the SE_T>15dB, and SE_T can be expressed as:

$$SE_T = SE_A + SE_R \quad (6)$$

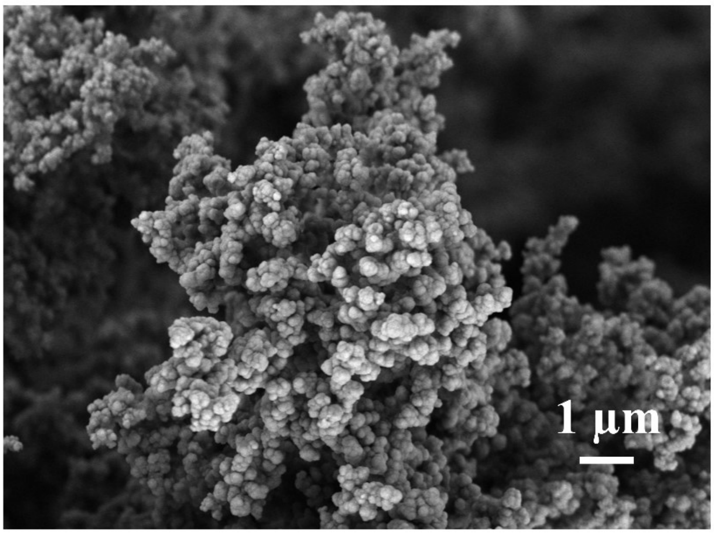

Fig. S1 SEM image of MF@PPy at high magnification.

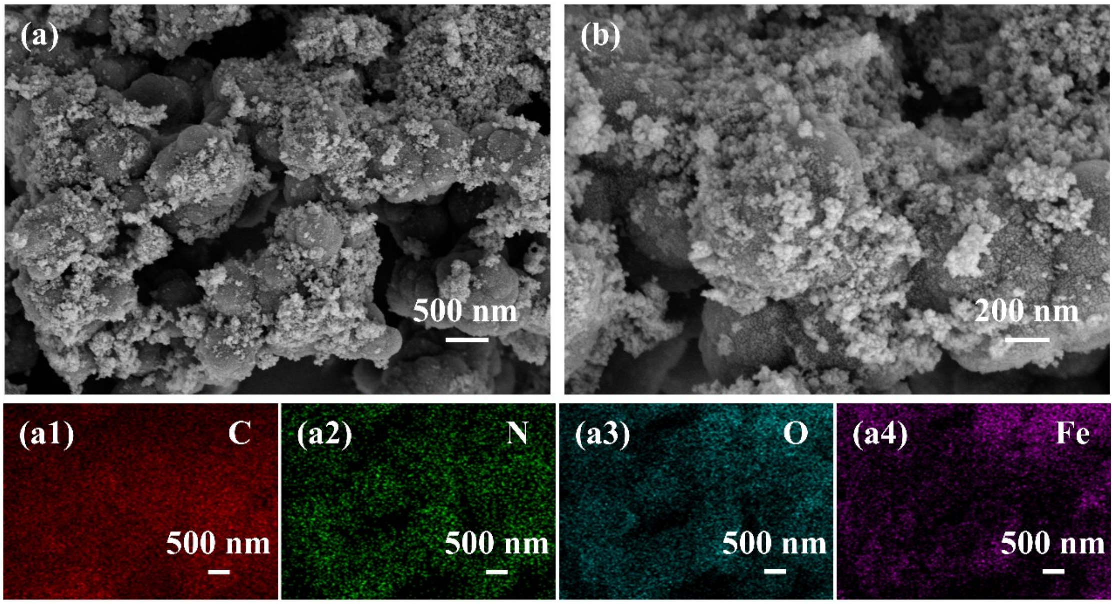

Fig. S2 (a, b) SEM images of PPy@Fe_3O_4 particles. (a1-a4) EDS mapping images of PPy@Fe_3O_4 particles.

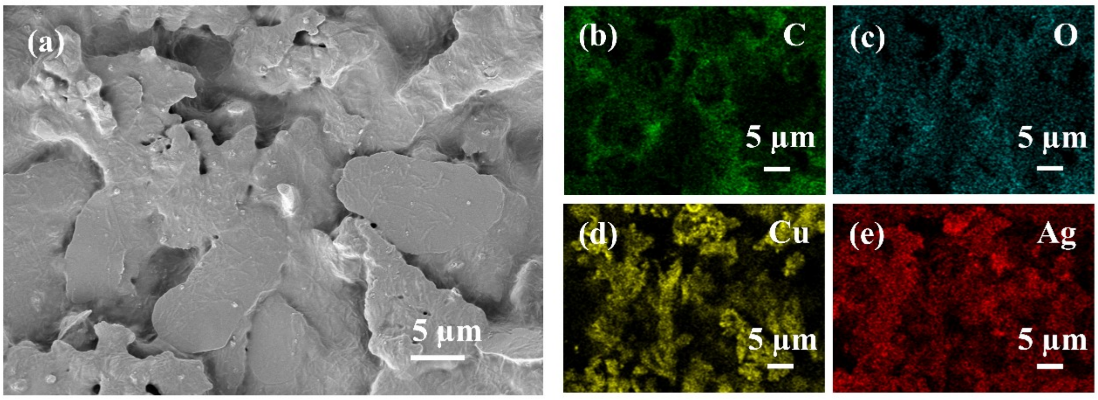

Fig. S3 (a) SEM image and (b-e) EDS mapping images of AgP.

Fig. S4 Optical image of $AgP/PDMS/Al_2O_3$ layer.

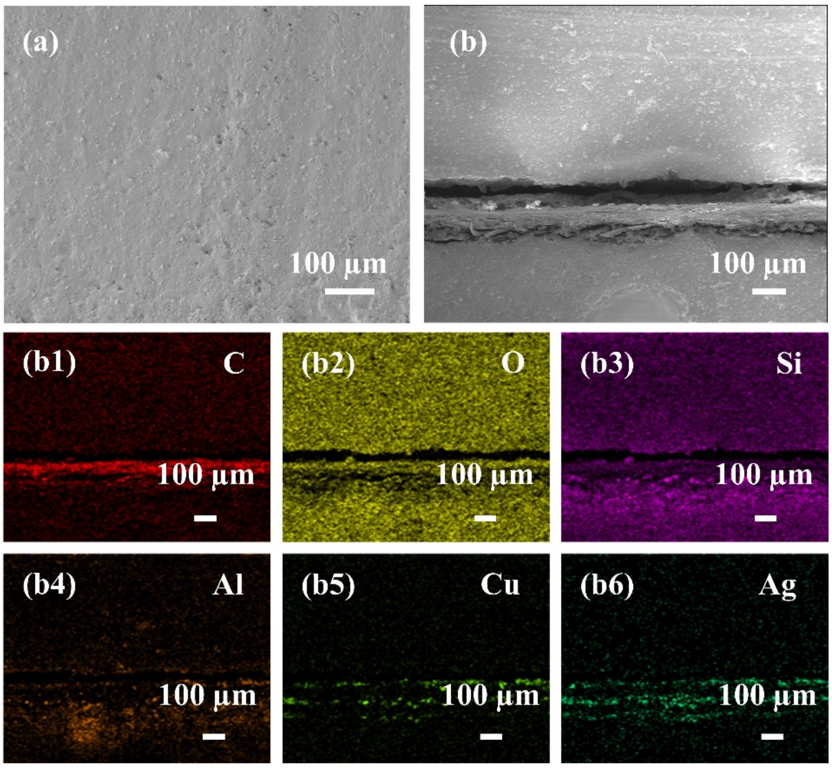

Fig. S5 (a) SEM image of the surface of the $AgP/PDMS/Al_2O_3$ layer. (b) SEM image of $AgP/PDMS/Al_2O_3$ layer cross sections. (b1-b6) EDS mapping images of $AgP/PDMS/Al_2O_3$ layer cross sections.

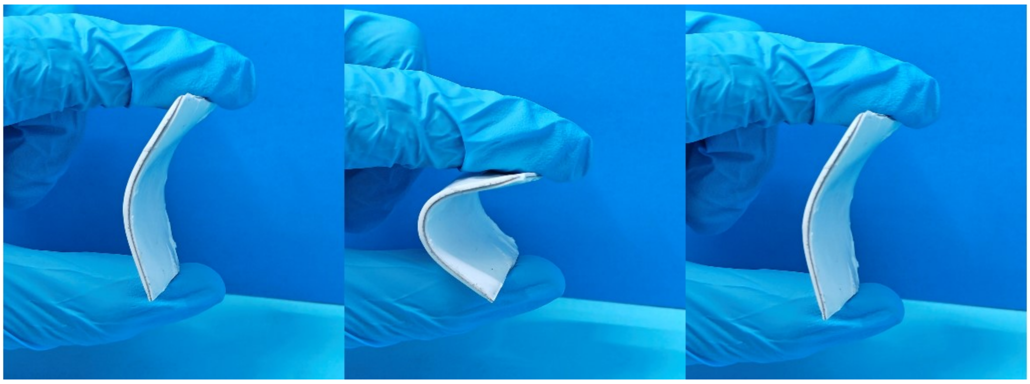

Fig. S6 Digital images of samples after bending 1000 times.

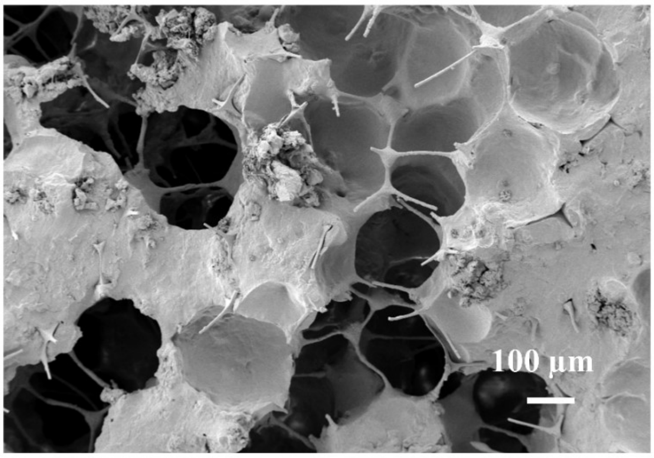

Fig. S7 SEM image of the MPF.

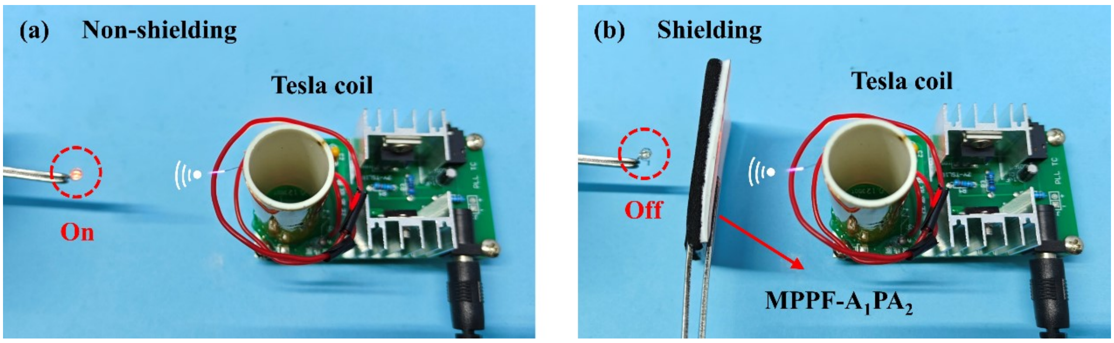

Fig. S8 A practical EMI shielding application measurement in a Tesla coil system with (a) non-shielding and (b) shielding.

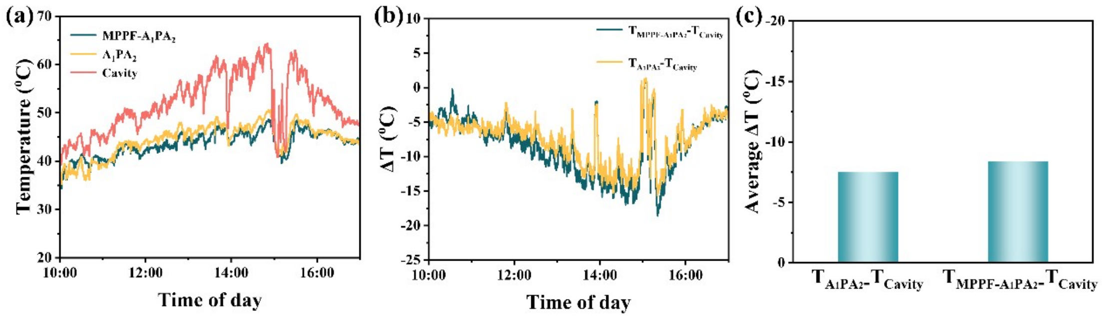

Fig. S9 (a) Real-time temperature profile, (b) temperature difference and (c) average temperature difference for MPPF-A_1PA_2 and A_1PA_2 outdoor cooling tests.

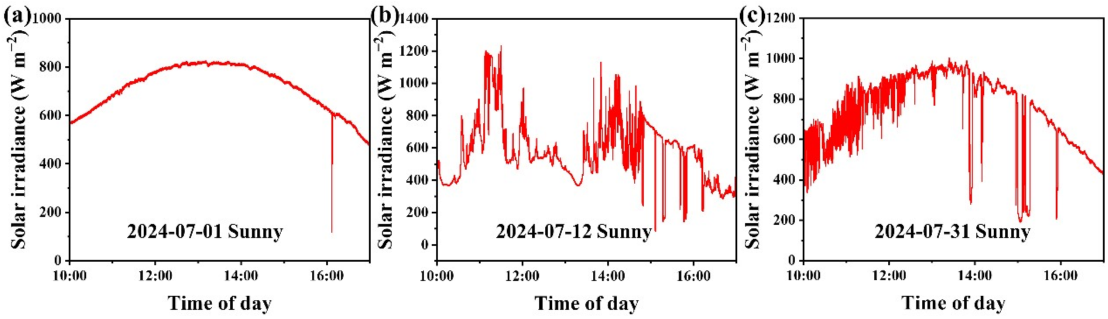

Fig. S10 Solar radiation intensity when (a) glass sheet, (b) Al sheet and (c) wood sheet are used as substrates.

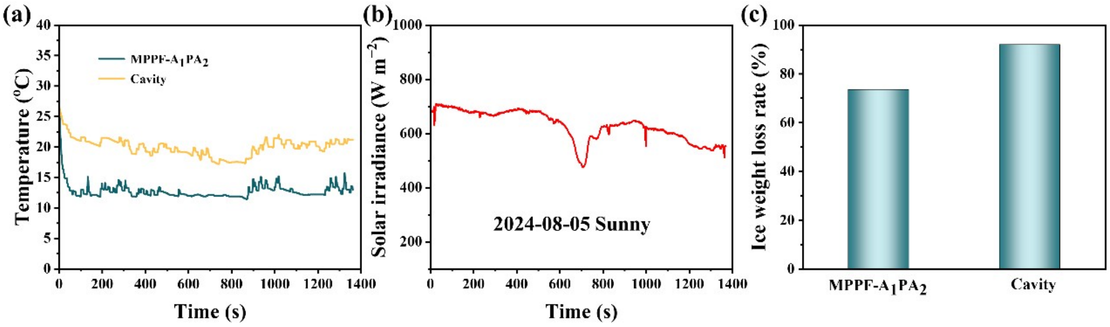

Fig. S11 (a) Real-time temperature profile, (b) solar radiation intensity and (c) ice cube weightlessness of MPPF-A_1PA_2 composite for ice melt retardation experiment.

Table S1 Comparison of EMI shielding properties of this work with other EMI shielding materials.

Samples	EMI SE (dB)	A	Reference
TPU/CNT/Ag	79.4	0.46	1
PF/Fe_3O_4@PPy/Cu	41.1	0.8	2
TPU/AgNR foam	35.5	0.915	3
MPP-MXene/CNF	47.2	0.972	4
Ni@MF-5/CNT-75/PBAT	38.3	0.19	5
VMQ/Fe_3O_4@MWCNT/Ag@NWF	90	0.46	6
NiM10/PCM	34.6	0.835	7
Ni@MF/CNT3/TSM/PDMS	45.3	0.72	8
rGO@Fe_3O_4/T-ZnO/Ag/WPU	87.2	0.61	9
VMQ/Ag@GF/MWCNT/Fe_3O_4	78.6	0.82	10
Sb_2O_3-Ni-MWCNTs/PDMS	54.4	0.51	11
Silicone rubber/Ag@HGMs/Fe_3O_4@MWCNTs	59.4	0.41	12
FA-CNF/MXene/FA-CNF	63.9	0.33	13
CNF-MXene composite aerogels	93.5	0.26	14
MXene/ANFs hybrid aerogel	56.8	0.09	15
MPPF-A_1PA_2	**65.0**	**0.79**	**This work**

Table S2 Comparison of cooling performances of the radiative cooling materials.

Materials	Year	Temperature drop (°C)	Solar irradiance (W m^{-2})	Reference
PDMS/Al_2O_3	2020	5	862	16
SiO_2/TiO_2/PDMS/Al	2022	5.3	523	17

$AlPO_4$/PDMS fabric	2020	5.4	998	18
Porous PDMS sponge	2021	4.6	900	19
PDMS/Al	2021	2.4	760	20
PMMA/SiO_2	2021	6.0-8.9	900	21
PDMS/PE aerogel	2020	5.0-6.0	1000	22
HDPE/Cr_2O_3/TiO_2	2021	7.0	1100	23
SiO_2@TiO_2/PDMS/Al	2022	6.9	1000	24
PVDF/$BaSO_4$/SiO_2	2021	5.1	803	25
SiO_2/Al	2021	7.3	633	26
$BaSO_4$/P(VDF-HFP)	2022	2.0	1000	27
MPPF-A_1PA_2		**8.7**	**713**	**This work**

Notes and references

1 B. Sun, S. Sun, P. He, H.-Y. Mi, B. Dong, C. Liu and C. Shen, *Chem. Eng. J.*, 2021, **416**, 129083.

2 W. Chu, J. Li, J. Lin, W. Li, J. Xin, F. Liu, X. He, Z. Ma and Q. Zhao, *Compos. Sci. Technol.*, 2024, **249**, 110489.

3 Z. Li, Y. Shen, Y. Zhou, B. Zhou, C. Liu and Y. Feng, *J. Mater. Sci. Technol.*, 2024, **197**, 9–16.

4 J. Tang, M. Fu, T. Zhang, T. Zuo, W. Feng, W. Wang and D. Yu, *Polymer*, 2024, **308**, 127354.

5 B. Xue, Y. Li, Z. Cheng, S. Yang, L. Xie, S. Qin and Q. Zheng, *Nano-Micro Lett.*, 2022, **14**, 16.

6 J. Yang, X. Liao, G. Wang, J. Chen, W. Tang, T. Wang and G. Li, *J. Mater. Chem. C*, 2020, **8**, 147–157.

7 H. Cheng, L. Xing, Y. Zuo, Y. Pan, M. Huang, A. Alhadhrami, M. M. Ibrahim, Z. M. El-Bahy, C. Liu, C. Shen and X. Liu, *Adv. Compos. Hybrid Mater.*, 2022, **5**, 755–765.

8 Q. Peng, M. Ma, Q. Chu, H. Lin, W. Tao, W. Shao, S. Chen, Y. Shi, H. He and X. Wang, *J. Mater. Chem. A*, 2023, **11**, 10857–10866.

9 Y. Xu, Y. Yang, D.-X. Yan, H. Duan, G. Zhao and Y. Liu, *ACS Appl. Mater. Interfaces*, 2018, **10**, 19143–19152.

10 J. Yang, X. Liao, G. Wang, J. Chen, P. Song, W. Tang, F. Guo, F. Liu and G. Li, *Compos. Sci. Technol.*, 2021, **206**, 108663.

11 Q.-M. He, J.-R. Tao, Y. Yang, D. Yang, K. Zhang, B. Fei and M. Wang, *Composites, Part A*, 2022, **156**, 106901.

12 J. Yang, X. Liao, G. Wang, J. Chen, F. Guo, W. Tang, W. Wang, Z. Yan and G. Li, *Chem. Eng. J.*, 2020, **390**, 124589.

13 Z. Guo, P. Ren, J. Wang, J. Tang, F. Zhang, Z. Zong, Z. Chen, Y. Jin and F. Ren, *Composites, Part B*, 2022, **236**, 109836.

14 H. Wang, Y. Jiang, Z. Ma, Y. Shi, Y. Zhu, R. Huang, Y. Feng, Z. Wang, M. Hong, J. Gao, L. Tang and P. Song, *Adv. Funct. Mater.*, 2023, **33**, 2306884.

15 Z. Lu, F. Jia, L. Zhuo, D. Ning, K. Gao and F. Xie, Composites, Part B, 2021, **217**, 108853.

16 T. Li, Y. Zhai, S. He, W. Gan, Z. Wei, M. Heidarinejad, D. Dalgo, R. Mi, X. Zhao, J. Song, J. Dai, C. Chen, A. Aili, A. Vellore, A. Martini, R. Yang, J. Srebric, X. Yin and L. Hu, *Science*, 2019, **364**, 760–763.

17 Y. Sun, M. Javed, Y. Ji, M. Z. Nawaz, Y. Wang, Z. Cai and B. Xu, *Sol. Energ. Mat. Sol. C.*, 2022, **245**, 111836.

18 S. Zhong, L. Yi, J. Zhang, T. Xu, L. Xu, X. Zhang, T. Zuo and Y. Cai, *Chem. Eng. J.*, 2021, **407**, 127104.

19 L. Zhou, J. Rada, H. Zhang, H. Song, S. Mirniaharikandi, B. S. Ooi and Q. Gan, *Adv. Sci.*, 2021, **8**, 2102502.

20 K. Lin, L. Chao, T. C. Ho, C. Lin, S. Chen, Y. Du, B. Huang and C. Y. Tso, *Energ. Buildings*, 2021, **252**, 111400.

21 T. Wang, Y. Wu, L. Shi, X. Hu, M. Chen and L. Wu, *Nat. Commun.*, 2021, **12**, 365.

22 M. Yang, W. Zou, J. Guo, Z. Qian, H. Luo, S. Yang, N. Zhao, L. Pattelli, J. Xu and D. S. Wiersma, *ACS Appl. Mater. Interfaces*, 2020, **12**, 25286–25293.

23 Z. Yang, T. Jiang and J. Zhang, *Sol. Energ. Mat. Sol. C.*, 2021, **219**, 110783.

24 D. Hu, S. Sun, P. Du, X. Lu, H. Zhang and Z. Zhang, *Composites, Part A*, 2022, **158**, 106949.

25 Z. Cheng, H. Han, F. Wang, Y. Yan, X. Shi, H. Liang, X. Zhang and Y. Shuai, *Nano Energy*, 2021, **89**, 106377.

26 L. Carlosena, Á. Andueza, L. Torres, O. Irulegi, R. J. Hernández-Minguillón, J. Sevilla and M. Santamouris, *Sol. Energ. Mat. Sol. C.*, 2021, **230**, 111209.

27 D. Han, J. Fei, J. Mandal, Z. Liu, H. Li, A. P. Raman and B. F. Ng, *Sol. Energ. Mat. Sol. C.*, 2022, **240**, 111723.